

Biosensor based on TiO₂ Nanofibers Prepared Using High Energy Electron Beam Treatment for Rapid and Efficient Glucose Determination

Zhitong Hu, Ju Rong, Zhaolin Zhan, Xiaohua Yu*

School of Materials Science and Engineering, Kunming University of Science and Technology, Kunming 650093, China

*E-mail: xiaohua_y@163.com

Received: 23 June 2019 / Accepted: 22 August 2019 / Published: 7 October 2019

TiO₂ nanofibers (p-TDNF) were synthesized by electrospinning and highly active TiO₂ nanofibers (m-TDNF) were obtained by electron beam treatment of p-TDNF and assessed for the enzyme immobilization and biosensing applications. Studies have shown surface defects and Ti³⁺ are formed on m-TDNF. Significantly, the better electron conduction properties were exhibited for glucose oxidase (GOD) immobilized on m-TDNF, and favorable electrocatalytic properties for glucose detection can be acquired. Impressively, GOD/m-TDNF/Nafion/GCE glucose biosensor exhibits high sensitivity of 12.5 $\mu\text{A}\cdot\text{mM}^{-1}\text{cm}^{-2}$ and low detection limit of 0.9 μM as well as excellent selectivity and stability. Moreover, the accurate glucose determination and good recoveries in human blood serum implied their enormous potentiality in the practical applications. These results indicate that the preparation of m-TDNF offers a novel idea for the development of glucose biosensors.

Keywords: TiO₂ nanofibers, high energy electron beam, surface defects, biosensor

1. INTRODUCTION

Fast and efficient glucose testing equipment is highly demanded nowadays of the growing population of people with diabetes [1-4]. Therefore, in order to improve the defects of conventional biosensors, developing glucose biosensors with high sensitivity, selectivity and stability from nanostructured materials is a major trend [5,6]. Among them, the direct electron transfer between the immobilized enzyme and the electrode is of great significance for the development of the enzymatic biosensors and has received extensive attention [7,8]. Furthermore, to solve the issues of direct electron transfer in enzymatic biosensors, all kinds of nanostructured materials such as metal nanoparticles [9], carbon nanotubes [10] and metal oxides [11] have wide range of applications in the development of biosensors. It can be seen that a biosensor with excellent performance can be designed according to

different characteristics of the material. Nevertheless, due to carbon nanomaterials, metal nanoparticles and metal oxides, respectively, have poor biocompatibility, high cost and low electrical conductivity, which limit their practical application.

Recently, TiO₂ nanofibers have been concerned extensively due to their good biocompatibility, high surface area and electrochemical applications [12-14]. As is known, the high surface-to-volume ratio of TDNF enables promote the interfacial charge carrier transfer rate [15]. TiO₂ nanofibers may facilitate electron transfer between the electrode and immobilized enzyme due to their unique physicochemical properties and offer an effect of electron-mediated [16]. However, the construction of high-quality electrochemical properties of nanostructured electrode materials is of vital importance for the ever-increasing demands of practical applications. The experimental results show that the electrocatalytic activity of titanium dioxide nanofibers is limited due to the quantum confinement effect [17]. Therefore, in order to promote the interaction between the enzyme and electrode, defect treatment of the TDNF has become a challenging problem.

Here, we offer a novel synthetic strategy of high sensitivity glucose biosensors based on electron beam induced TiO₂ nanofibers. TDNF with a high specific surface area was prepared by electrospinning and subjected to electron beam treatment. Among them, a large amount of surface defects and Ti³⁺ are generated on the TDNF by electron beam treatment. Therefore, compared to the pristine TDNF, these surface defects and Ti³⁺ cause the significant improvements of the material surface adsorption activity and band gap width. Interestingly, because of the unique structural characteristics of the p-TDNF surface, it creates conditions for excellent direct electron transfer between GOD and electrode.

2. MATERIALS AND METHODS

2.1 Materials

Tetrabutyl titanate (TBT), polyvinylpyrrolidone (PVP, M_w=1300000) and glucose oxidase (GOD, 200 units/mg), fructose (Fru), uric acid (UA), ascorbic acid (AA) and dopamine (DA) were purchased from Sigma-Aldrich (St.Louis). Phosphate buffer solution (PBS) is composed of Na₂HPO₄ and NaH₂PO₄. Chemicals and reagents such as acetone, ethanol, NH₄F, NaCl are of analytical grade.

2.2 Preparation of TDNF

TBT (20 g) was dissolved in absolute ethanol (30 mL) under magnetic stirring at room temperature. PVP (15 g) was weighed and added to the TBT solution. The electrospinning precursor solution was obtained by placing the mixed solution magnetic stirring for 10 h. The electrospinning precursor was pumped by an injector pump (LSP01-3A) at a rate of 1.0 mL/h, and the detailed parameters were as follows: the applied voltage was 15 kV, the collection time and distance were 15 min and 15 cm, respectively. The samples were calcined at 500°C (argon atmosphere) for 2 h with the heating rate of 0.5°C/min.

Then, the prepared TDNF were treated by high-energy electron beam with a total exposure of 90 kGy under ambient conditions. TDNF before and after electron beam treatment were labeled as p-TDNF and m-TDNF, respectively.

2.3 Preparation of glucose biosensor

The glassy carbon electrode (GCE) was polished with a suspension of 0.05 μm $\alpha\text{-Al}_2\text{O}_3$ and washed with distilled water, nitric acid, acetone and distilled water, and dried with N_2 . Enzyme immobilization was implemented by immersing 10 mg TDNF in 5 mL 10 $\text{mg}\cdot\text{mL}^{-1}$ GOD solution fabricated in 0.1 M PBS (pH 7.0). The 5 μL 10 $\text{mg}\cdot\text{mL}^{-1}$ above mixed solution and the 10 μL 5% Nafion were sequentially dispensed onto the surface of the prepared GCE electrode, respectively, and dried in Nitrogen to form a TDNF/GOD/Nafion/GCE electrode.

2.4 Characterization

The crystalline structure of TDNF were analyzed by X-ray diffractometry (XRD, D/MAX-3B). TDNF microstructure was observed using SEM (VEGA-3SBH) and TEM (JEM-2100F). Raman spectra were collected by a Raman microprobe with 514 nm (Bruker, RENISHAW). The elemental valence of the TDNF was determined by X-ray photoelectron spectroscopy (XPS, PHI-5000 Versa Probe II). UV-Vis absorption spectra of samples were determined using spectrophotometer (TU-1901). PL spectra of samples were analyze by the He–Cd laser (HCL-40(I), Plasma). The structural characteristics of the samples were detected by electron paramagnetic resonance (EPR, Bruker A300). Enzyme immobilization was investigated by FTIR (Nicolet6700, Thermo Fisher Scientific). The electrochemical measurements were performed on an electrochemical workstation (CHI 760E).

3. RESULTS AND DISCUSSION

The surface morphology and microstructure of TDNF before and after electron beam modification are shown in Figs. 1a and b. Figure 1a shows that p-TDNF has a diameter of around 120 nm and the length of a single root exceeds 10 μm . The morphologies and structure of m-TDNF (Fig. 1b) were not changed after the electron beam modification. According to the TEM image (Fig. 1c), the diameter of m-TDNF was in the range of 100 to 120 nm. Figure 1d shows that the lattice spacing of m-TDNF was 0.37 nm, which was consistent with the distance during the (101) plane of the anatase TiO_2 . Meanwhile, the phase composition of p-TDNF and m-TDNF were also determined by XRD. The XRD diffraction patterns of p-TDNF shows sharp peaks at 25.3, 37.8, 48.1, 53.9, 55.1 and 62.7 degrees (Fig. 1e), which correspond to the (101), (004), (200), (105), (211) and (204) planes of the anatase TiO_2 structure (JCPDS no.21-1272). Compared with p-TDNF, the diffraction peak of m-TDNF is slightly reduced, which may because of surface vacancy of m-TDNF [18]. There are not apparent signs of any impurity detected by XRD, indicating that the basic structure of TiO_2 has not changed after electron

beam irradiation. According to the Scherrer-Wilson equation [19], the average grain sizes of the p-TDNF and m-TDNF are 20.8 and 21.2 nm, respectively.

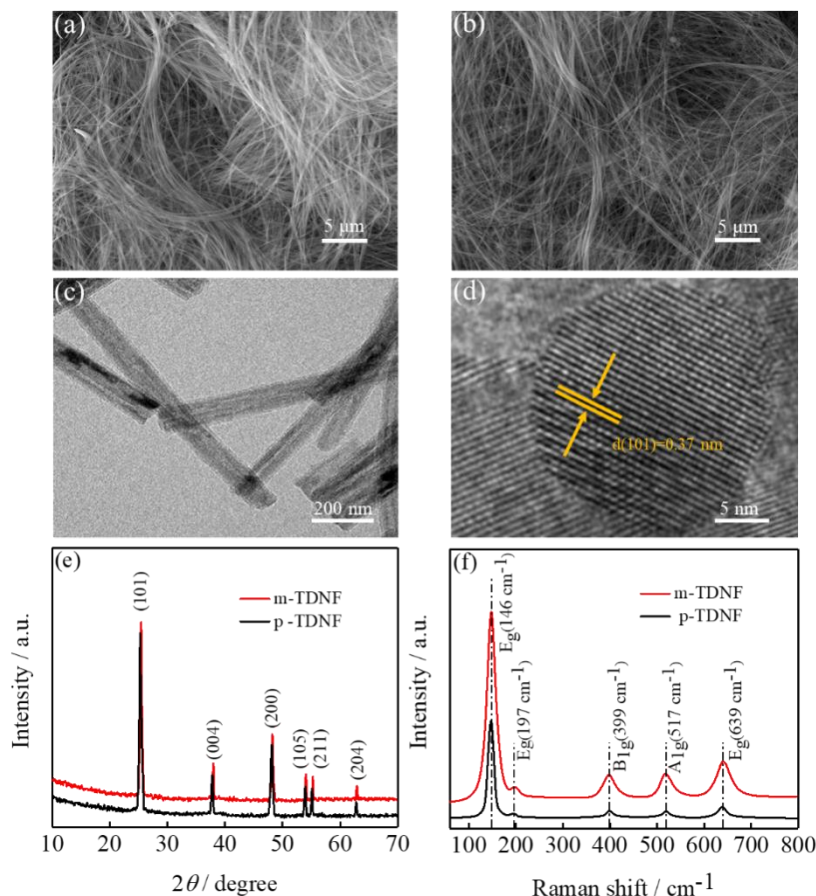


Figure 1. (a) SEM images of p-TDNF; (b) SEM images of m-TDNF; (c) TEM images of m-TDNF; (d)HRTEM images of m-TDNF; (e) XRD patterns, and (f) Raman spectra of the p-TDNF and m-TDNF nanoparticles.

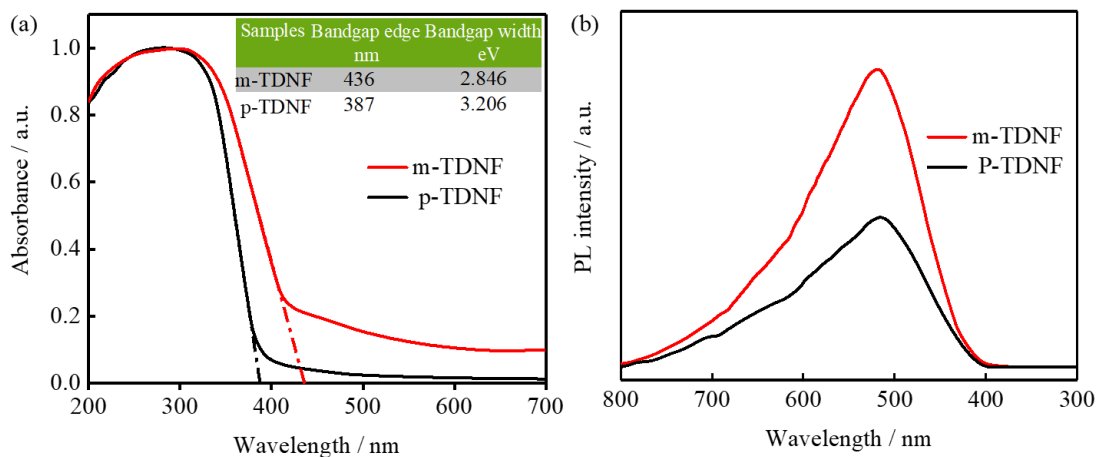


Figure 2. (a) UV-vis diffuse absorbance and (b) PL spectra of the p-TDNF and m-TDNF.

There is a slight increase of the grain size due to irradiation with electron beam, suggesting that defects at the surface of m-TDNF were formed. To further understand the structural properties of the samples, p-TDNF and m-TDNF Raman spectroscopy were analyzed. Figure 1f shows the Raman spectra of p-TDNF and m-TDNF, and the vibrational absorption peaks at 146, 197, 399, 517 and 639 cm^{-1} correspond to anatase TiO_2 [20]. Interestingly, compared to p-TDNF, the peak of m-TDNF is broadened due to the formation of defects or Ti^{3+} after electron beam irradiation [21].

Electron beam irradiation of the TDNF cause surface defects. Hence, a change in the rate of electron transport of samples is predictable. Figure 2a displays the UV/Vis spectra absorption of p-TDNF and m-TDNF. Owing to the existence of Ti^{3+} and surface defects, the bandgap width of m-TDNF is 2.846 eV, which is 0.36 eV lower than p-TDNF, which reduces the transmission barrier and increases the electron diffusion path [22,23]. Since the band gap narrowing is proportional to the rate of electron transport, it is expected that the m-TDNF electrode exhibits better electron conduction characteristics. Therefore, m-TDNF was used as a mediator between the electrode and enzyme in the biosensors. To further understand the effectiveness of transfer of charge carriers, p-TDNF and m-TDNF PL spectra were analyzed (Fig. 2b). It is worth noting, compared to p-TDNF, m-TDNF displayed a higher PL intensity. Due to the existence of surface defects in m-TDNF, which results in a change in their chemical properties. Studied by Naldoni [24] and Santara [25] have shown that the PL signal can appear easily due to more sensitive properties of excitons to surface defects. Thus, the m-TDNF has high intensity of the PL spectrum for the presence of the surface defects [23,26].

To get more information about the p-TDNF and m-TDNF, the EPR spectra are shown in Fig. 3a. Under low temperature, many defect-related species and vacancies in TDNF can be detected. As can be seen, compared with p-TDNF, m-TDNF displays a strong EPR signal at $g=2.003$, which is due to the capture of electrons at the oxygen vacancies, thus it verifies the presence of Ti^{3+} on the m-TDNF surface [27]. Hence, it demonstrates the paramagnetic nature of the m-TDNF which further enhances the electrochemical activity of the material surface [18]. In order to further analyze the effect of electron beam on the surface characterization of the samples, the XPS spectra of p-TDNF and m-TDNF are shown in Figs. 3b-f. Figure 3b shows that both p-TDNF and m-TDNF consist of Ti, O and C elements, where C element is caused by contamination [28]. It can be seen that the peaks with binding energies at 458.52, 458.75, 464.18 and 464.20 eV represent Ti^{4+} ; the peaks at 456.28 and 461.80 eV represent Ti^{3+} (Figs. 3c and 3e). Significantly, Ti^{3+} appears in m-TDNF compared to p-TDNF. Meanwhile, the peaks with binding energies at 530.68 and 530.69 eV represent O^{2-} ; the peaks at 532.24 and 532.28 eV represent OH^- . The O1s XPS spectra of p-TDNF and m-TDNF are shown in Figs. 3d and 3f, respectively. As can be seen, the peaks represented by O^{2-} and OH^- do not apparently shift, indicating that the surface species of the sample undergo no change under electron beam treatment. More importantly, the presence of Ti^{3+} and surface defects on the surface of m-TDNF can inhibit the recombination of electron-hole pairs and enhance chemical activity [18].

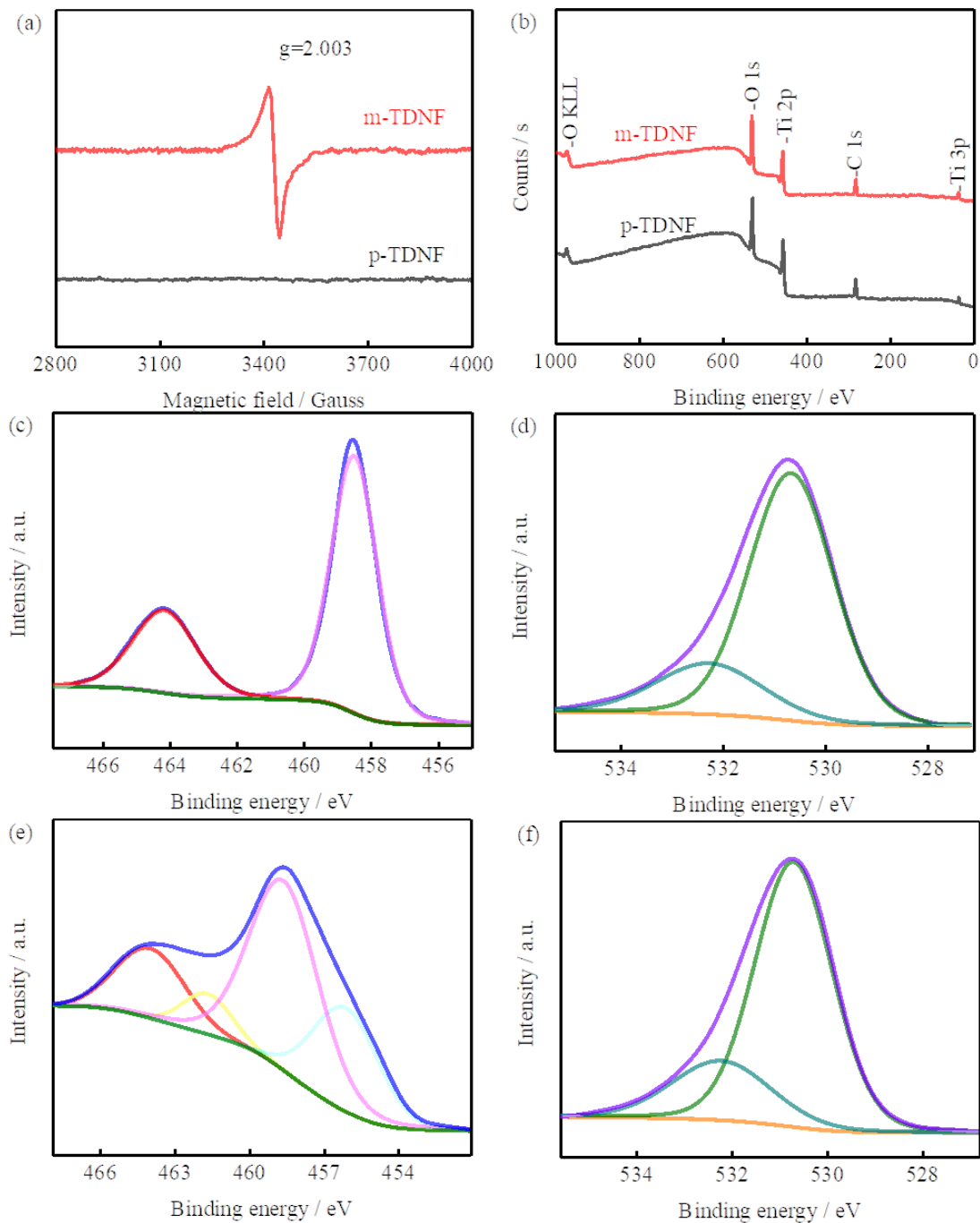


Figure 3. (a) EPR and (b-f) XPS spectra analysis of p-TDNF and m-TDNF.

The effectiveness of enzyme immobilization on p-TDNF and m-TDNF were determined by FT-IR spectroscopy (Fig. 4) to investigate the immobilization of enzymes. The GOD display three characteristic peaks at 1658, 1544 and 1103 cm^{-1} , corresponding to the typical amide I, amide II adsorption bands and the C–O bond stretching vibration of GOD, respectively (Fig. 4a) [29]. Both p-TDNF and m-TDNF have signal peaks at 1635 and 1040 cm^{-1} , which correspond to the vibration of the H–O–H bond and Ti–O–C bond, respectively [30].

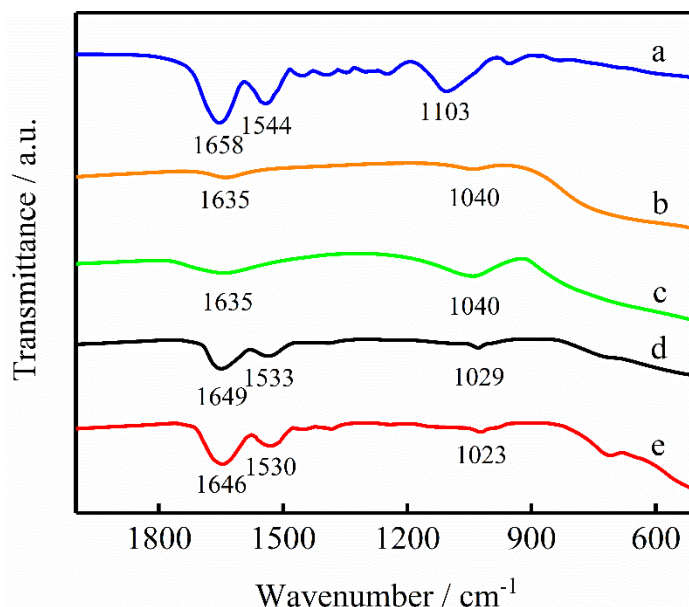


Figure 4. FT-IR spectra of GOD (a), p-TDNF (b), m-TDNF (c), GOD/p-TDNF (d) and GOD/m-TDNF (e).

However, compared with P-TDNF, the adsorption peak in m-TDNF is higher, indicating that the effects of H-O-H and Ti-O-C bonds were enhanced after electron beam irradiation. The presence of both amide I and II adsorption peaks in the spectrum of GOD/p-TDNF and GOD/m-TDNF implies that the enzyme adsorbed on the surface of TiO₂. Significantly, the peaks of amide adsorption in GOD/p-TDNF and GOD/m-TDNF were reduced to 1649, 1533 cm⁻¹ and 1646, 1530 cm⁻¹, respectively, may owing to the strong electrostatic interaction between the immobilized enzyme and TiO₂ [31]. Moreover, the adsorption peak of Ti-O-C in GOD/p-TDNF and GOD/m-TDNF have decreased, confirming the electrostatic interaction between the GOD and the TDNF. Therefore, the above results indicate the effective immobilization of GOD enzyme molecules on the TDNF surface.

To study the electrochemical behavior of the different electrode materials, electrocatalytic experiments were carried out on the GOD/Nafion/GCE, m-TDNF/Nafion/GCE and GOD/m-TDNF/Nafion/GCE electrodes. Figure 5a shows the CVs obtained at different electrodes in 0.1 M PBS solution (pH 7.0) at scan rate of 100 mV s⁻¹. The GOD/Nafion/GCE and m-TDNF/Nafion/GCE electrodes only exhibit typical capacitive CVs responses caused by their double layer capacitance without any obvious redox peaks (Fig. 5a), indicating that both the GOD/Nafion/GCE and m-TDNF/Nafion/GCE are electro-inactive over this potential range. As can be seen, compared with the GOD/p-TDNF/Nafion/GCE electrode, the GOD/m-TDNF/Nafion/GCE electrode displays the obvious redox peaks whose anodic and cathodic peak potential at -0.413 and -0.465 V respectively. Significantly, the anode and cathode response currents of GOD/m-TDNF/Nafion/GCE were 1.6 times higher than that of GOD/p-TDNF/Nafion/GCE. This phenomenon is due to the strong interaction of GOD with p-TDNF, indicating that electron beam treatment enhances direct electron transfer between the GOD and p-TDNF. In addition, Figure 5b shows the CVs of the GOD/m-TDNF/Nafion/GCE were conducted in PBS containing 0, 0.5, 1, 2 and 5 mM of glucose. Interestingly, the redox peak current decreases as the glucose concentration increases (Fig. 5b), indicating that oxygen reduction occurs on the GOD/m-

TDNF/Nafion/GCE electrode. This implies that GOD/m-TDNF/Nafion/GCE electrode exhibits high electrocatalytic performance, which makes the determination of glucose.

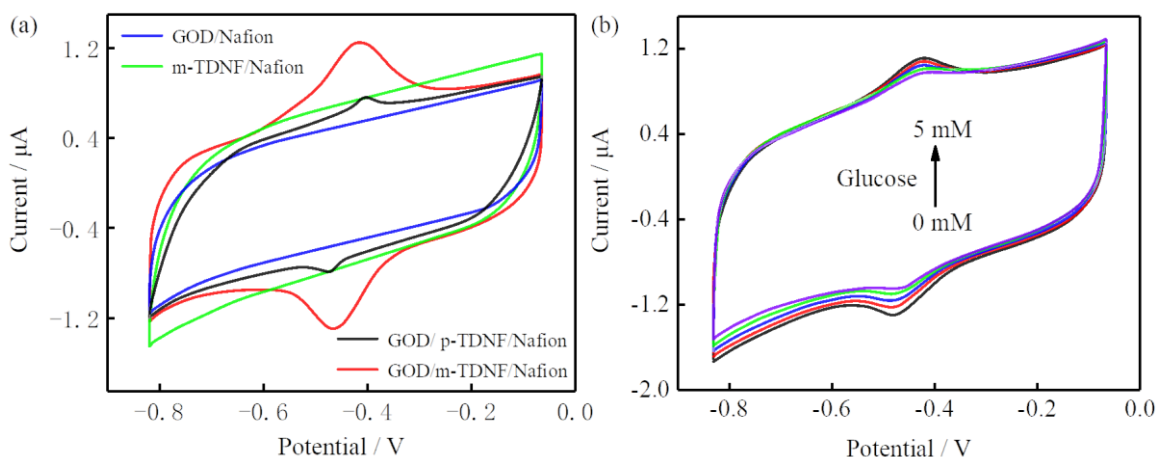


Figure 5. (a) CVs of GOD/Nafion/GCE, m-TDNF/Nafion/GCE, GOD/p-TDNF/Nafion/GCE and GOD/m-TDNF/Nafion/GCE in 0.1 M PBS solution (pH 7.0) at scan rate of 100 mV s^{-1} . (b) CVs of the GOD/TDNF/Nafion/GCE in 0.1 M PBS solution (pH 7.0) including 0, 0.5, 1, 2 and 5 mM glucose at a scan rate of 100 mV s^{-1} .

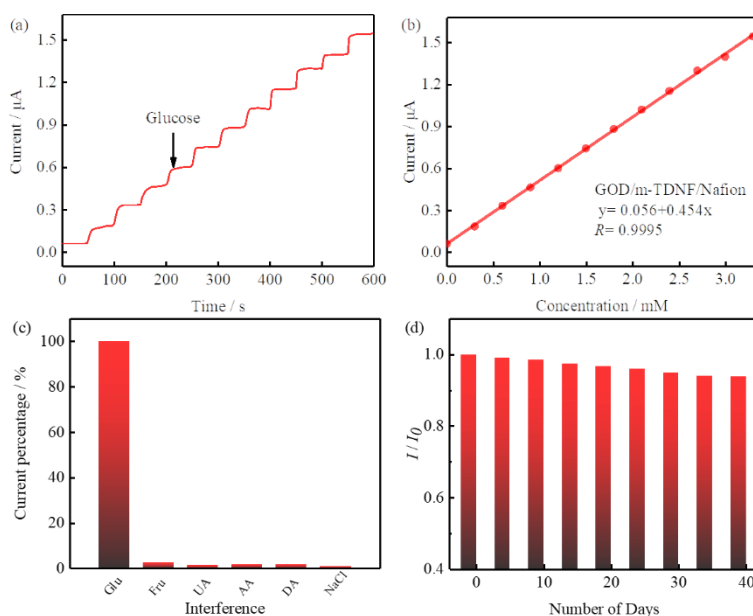


Figure 6. (a) Amperometric response of GOD/m-TDNF/Nafion/GCE glucose sensors in 0.1 M PBS with consecutive addition of various concentrations of glucose, (b) Linear fitting curve between current and glucose concentrations, (c) Effect of interfering species to the response and (d) Long-term stability of the GOD/m-TDNF/Nafion/GCE glucose biosensors.

In order to further assess the analytical performance of GOD/m-TDNF/Nafion/GCE sensors, the experiment of amperometric current–time were performed. Figure 6a displays the amperometric

response of GOD/m-TDNF/Nafion/GCE electrode with continuous addition of glucose to 0.1 M PBS (pH 7) at 0.5V. As can be seen, as the glucose concentration increases, the current increases rapidly and shows a fast response time of less than 3 s, revealing the rapid response and sensitive of GOD/m-TDNF/Nafion/GCE to glucose oxidation. In addition, the amperometric response current on the GOD/m-TDNF/Nafion/GCE electrode increased linearly with glucose concentrations between 5 μ M and 3.3 mM as shown in Fig. 6b. The linear fitting equations for the current density and glucose concentration of the GOD/m-TDNF/Nafion/GCE electrodes are shown in equations:

$$I=0.056+0.454C$$

where I represent the response current, C represent the glucose concentration.

Meanwhile, the limit of detection (LOD) and sensitivity have been calculated to be 0.9 μ M (S/N=3) and 12.5 μ A \cdot mM⁻¹cm⁻², respectively. The sensitivity, linear range and response time values obtained for GOD/m-TDNF/Nafion/GCE are comparable with or better than those of metal oxide-based glucose sensors as shown in Table 1.

Table 1. Electrochemical performance of various metal oxide-based glucose biosensors.

Electrode material	Sensor sensitivity (mA \cdot Mm ⁻¹ \cdot cm ⁻²)	Linear range (mM)	Response time (s)	Ref
GOD/m-TDNF/Nafion/GCE	12.5	0.005-3.3	<3	This work
GOD/1DHS TiO ₂ /Nafion/GCE	9.9	0.05-1.5	<5	[5]
GOD/mesoporous TiO ₂	3.9	0.15-1.2	<10	[30]
GOD/NiO hollow spheres	3.4	1.5-7	<8	[32]
GOD/nanocrystalline TiO ₂	4.6	0-3	<30	[33]
GOD/TiO ₂ -copolymer	2.3	0-9	<20	[34]

The GOD/m-TDNF/Nafion/GCE glucose sensors also exhibit excellent selectivity and stability for glucose detection. We investigated amperometric responses with continuous addition of glucose, Fru, UA, AA, DA, NaCl and glucose in 0.1 M PBS under a working voltage of 0.5 V and a time interval of 50 s. In the presence of interfering species, the electrochemical response of glucose is shown in Fig. 6c. It can be seen that the addition of interfering species such as Fru, UA, AA, DA and NaCl made response currents less than 4%, suggesting the high selectivity of GOD/m-TDNF/Nafion/GCE in the determination of glucose.

Meanwhile, in order to further verify the long-term stability of the GOD/m-TDNF /Nafion/GCE glucose sensor, the current response of 1 mM glucose was detected every 5 days, and the biosensor is stored in the refrigerator with the temperature of 4°C. Figure 6d shows a 93.8% current response even after 40 days, displaying the good storage stability of the GOD/m-TDNF/ Nafion/GCE glucose

biosensor. This is because the TDNF surface after the electron beam treatment provides more active sites for GOD immobilization, to further facilitate the strong electrostatic interaction between GOD and m-TDNF.

Equally importantly, GOD/m-TDNF/Nafion/GCE glucose biosensor was utilized for determination of glucose in human serum samples by implementing standard addition method. The human serum samples were obtained from hospitalized patients, and measured its glucose concentration of 5 mM. In order to verify the accuracy of the GOD/m-TDNF/Nafion/GCE biosensor for measuring serum glucose level, 2 mL of serum was diluted to 10 mL by the addition of PBS (pH 7). The amperometric experiments were implemented to study the glucose oxidation at GOD/m-TDNF/Nafion/GCE biosensor.

Table 2. Analysis of glucose in human serum.

Samples	Added (mM)	Found (mM)	RSD (%)	Recovery (%)
1	0.1	1.098	2.2	99.8
2	0.2	1.241	2.4	103.4
3	0.5	1.502	2.3	100.1
4	1	1.992	2.1	99.6
5	2	2.991	2.5	99.7

Table. 2 shows the recovery values for the GOD/m-TDNF/Nafion/GCE electrode are in the range from 99.6 to 103.4%. Thus, the GOD/m-TDNF/Nafion/GCE glucose biosensor provides the excellent practical feasibility for accurate determination of glucose in real samples.

4. CONCLUSIONS

In summary, the p-TDNF was easily prepared by electrospinning and fabricated highly active m-TDNF under electron beam induction. Interestingly, the electron beam treatment provides more active sites for enzyme immobilization on the surface of p-TDNF and to the strong electrostatic interaction between the GOD and m-TDNF. It is worth noting that the GOD/m-TDNF/Nafion/GCE glucose biosensor has excellent electrocatalytic performance. Moreover, the developed GOD/m-TDNF/Nafion/GCE glucose biosensor also showed good analytical properties such as high sensitivity of $12.5 \mu\text{A}\cdot\text{mM}^{-1}\text{cm}^{-2}$, low LOD of $0.9 \mu\text{M}$ and fast current response within 3 s as well as favorable selectivity and long-term stability. More importantly, the practical application of GOD/m-TDNF/Nafion/GCE glucose biosensor in human serum showed good recoveries. In addition, the Surface defects generated by Electron beam induction may introduce more interesting properties, including photocatalysis and electrochemistry, into the p-TDNF.

References

1. M. Baghayeri, H. Veisi and M. Ghanei-Motlagh, *Sensor. Actuat. B-Chem.*, 249 (2017) 321-330.

2. Z. Kang, K. Jiao, X. Xu, R. Peng, S. Jiao and Z. Hu, *Biosens. Bioelectron.*, 96 (2017) 367-372.
3. Y. Song, M. Xu, C. Gong, Y. Shen, L. Wang, Y. Xie and L. Wang, *Sensor. Actuat. B-Chem.*, 257 (2018) 792-799.
4. N. Muthuchamy, R. Atchudan, T.N.J.I. Edison, S. Perumal and Y.R. Lee, *J. Electroanal. Chem.*, 816 (2018) 195-204.
5. P. Si, S. Ding, J. Yuan, X.W. Lou and D.H. Kim, *Acs Nano*, 5 (2011) 7617-7626.
6. Z. Yang, Y. Tang, J. Li, Y. Zhang and X. Hu, *Biosens. Bioelectron.*, 54 (2014) 528-533.
7. S.Y. Deng, G.Q. Jian, J.P. Lei, Z. Hu and H.X. Ju, *Biosens. Bioelectron.*, 25 (2009) 373-377.
8. C.S. Shan, H.F. Yang, J.F. Song, D.X. Han, A. Ivaska and L. Niu, *Anal. Chem.*, 81 (2009) 2378-2382.
9. K. Mondal, M.A. Ali, C. Singh, G. Sumana, B.D. Malhotra and A. Sharma, *Sensor. Actuat. B-Chem.*, 246 (2017) 202-214.
10. S. Kumar, W. Ahlawat, R. Kumar and N. Dilbaghi, *Biosens. Bioelectron.*, 70 (2015) 498-503.
11. L. Wu, S. Wu, Z. Xu, Y. Qiu, S. Li and H. Xu, *Biosens. Bioelectron.*, 80 (2016) 59-66.
12. M. Ghosh, M. Lohrasbi, S.S. Chuang and S.C. Jana, *ChemCatChem*, 8 (2016) 2525-2535.
13. M.J. Tian, F. Liao, Q.F. Ke, Y.J. Guo and Y.P. Guo, *Chem. Eng. J.*, 328 (2017) 962-976.
14. M.S. Jo, G.D. Park, Y.C. Kang and J.S. Cho, *Nanoscale*, 10 (2018), 13539-13547.
15. H.L. Hou, F.M. Gao, L. Wang, M.H. Shang, Z.B. Yang, J.J. Zheng and W.Y. Yang, *J. Mater. Chem. A*, 4 (2016) 6276-6281.
16. J. Zhang, M. Feng and H. Tachikawa, *Biosens. Bioelectron.*, 22 (2007) 3036-3041.
17. G. Žerjav, M.S. Arshad, P. Djinović, I. Junkar, J. Kovač, J. Zavašnik and A. Pintar, *Nanoscale*, 9 (2017) 4578-4592.
18. X. Liu, S. Gao, H. Xu, Z. Lou, W. Wang, B. Huang and Y. Dai, *Nanoscale*, 5 (2013) 1870-1875.
19. H.P. Klug and L.E. Alexander, *Wiley-VCH*, (1974) 992.
20. X. Chen, L. Liu, Y.Y. Peter and S.S. Mao, *Science*, 331 (2011) 746-750.
21. M.M. Khan, S.A. Ansari, D. Pradhan, M.O. Ansari, J. Lee and M.H. Cho, *J. Mater. Chem. A*, 2 (2014) 637-644.
22. Y. Yan, T. Lei, Y. Jiao, C. Wu and J. Xiong, *Electrochim. Acta*, 264 (2018) 20-25.
23. X. Pan, M.Q. Yang, X. Fu, N. Zhang and Y.J. Xu, *Nanoscale*, 5 (2013) 3601-3614.
24. A. Naldoni, M. Allieta, S. Santangelo, M. Marelli, F. Fabbri, S. Cappelli and V. Dal Santo. *J. Am. Chem. Soc.*, 134 (2012) 7600-7603.
25. B. Santara, P.K. Giri, K. Imakita and M. Fujii, *J. Phys. Chem. C*, 117 (2013) 23402-23411.
26. J. Liqiang, Q. Yichun, W. Baiqi, L. Shudan, J. Baojiang, Y. Libin, and S. Jiazhong, *Sol. Energ. Mat. Sol C.*, 90 (2006) 1773-1787.
27. S. Wang, L. Pan, J.J. Song, W. Mi, J.J. Zou, L. Wang and X. Zhang, *J. Am. Chem. Soc.*, 137 (2015) 2975-2983.
28. J. Fang, F. Wang, K. Qian, H. Bao, Z. Jiang and W. Huang, *J. Phys. Chem. C*, 112(2008) 18150-18156.
29. S. Wu, H.X. Ju and Y. Liu, *Adv. Funct. Mater.*, 17 (2007) 585-592.
30. S.J. Bao, C.M. Li, J.F. Zang, X.Q. Cui, Y. Qiao and J. Guo, *Adv. Funct. Mater.*, 18 (2008) 591-599.
31. J.H. Pazur and K. Kleppe, *Biochemistry*, 3 (1964) 578-583.
32. C. Li, Y. Liu, L. Li, Z. Du, S. Xu, M. Zhang, X.M. Yin and T.H. Wang, *Talanta*, 77 (2008) 455-459.
33. Q. Li, G. Luo, J. Feng, Q. Zhou, L.I. Zhang and Y. Zhu, *Electroanal.*, 13 (2001) 413-416.
34. X. Chen and S. Dong, *Biosens. Bioelectron.*, 18 (2003) 999-1004.